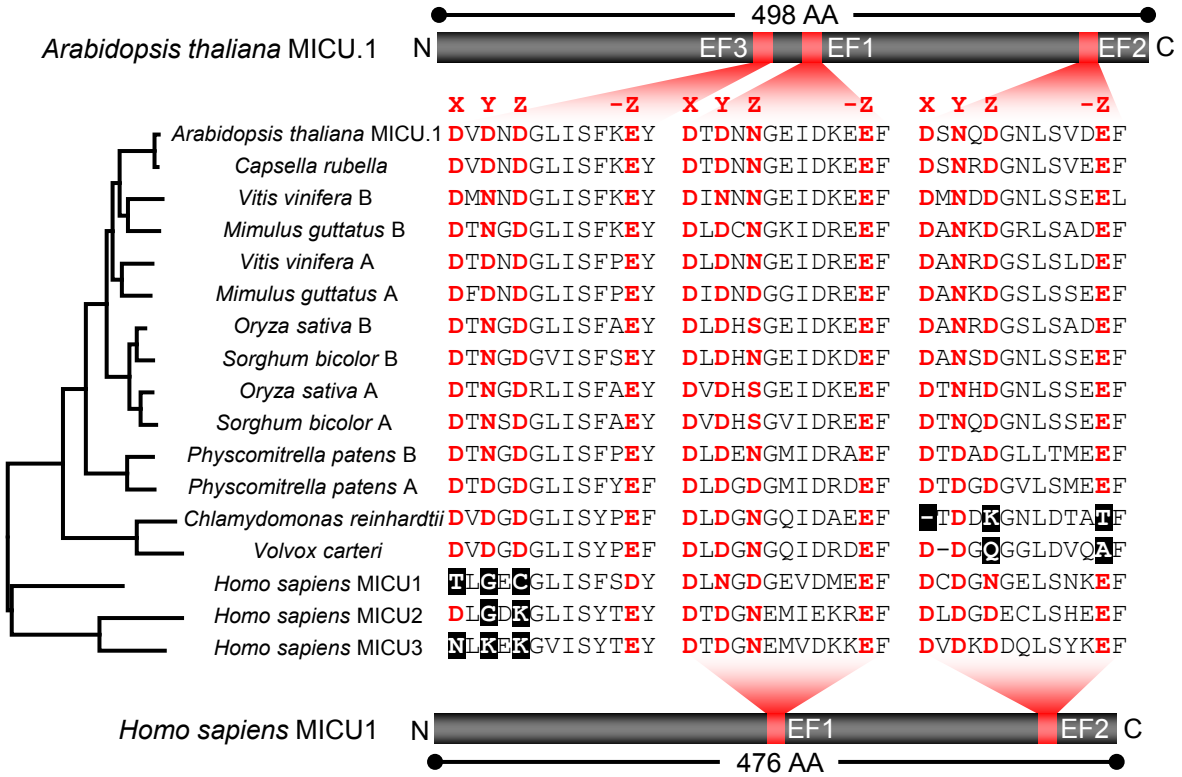

Supplemental Figure 1. Predicted features of At-MICU. (A) Conservation of EF hands in plant MICU homologues. Sequences of human MICU family proteins and their homologues from representative plant species were aligned using MUSCLE (Edgar, 2004; **Supplemental Data Set 1, Supplemental File 1**). Conservation is shown for the Ca^{2+}-coordinating loop of EF hand motifs present in human MICU1 (EF 1 & 2; Perocchi et al., 2010) and a third EF hand (EF3) predicted in all analysed land plant sequences. Side chains at positions X, Y, Z and -Z are critical for Ca^{2+} binding and boxed black if different from the canonical EF hand (Lewit-Bentley and Rety, 2000).

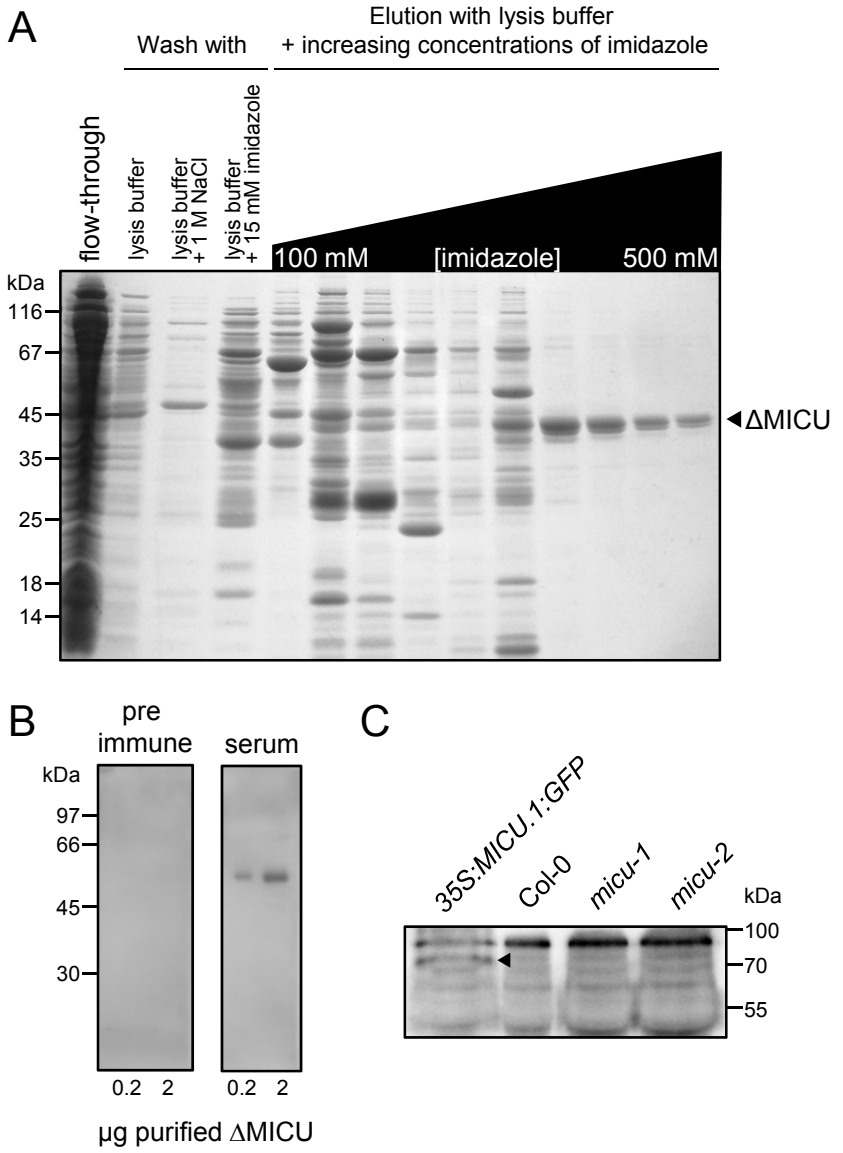

Supplemental Figure 2. Purification of ΔMICU and immunoblot with At-MICU antibody. (A) Purification of recombinant ΔMICU. *E. coli* ArcticExpress DE3 (Agilent Technologies) or *E. coli* Rosetta(DE3) cells expressing His:ΔMICU were lysed in lysis buffer (25 mM Tris, 150 mM NaCl, 5 % (v/v) glycerol, 0.1 mM DTT, pH 7.5) and soluble proteins were loaded onto a Ni^{2+} chromatography column (GE Healthcare) following centrifugal separation of cell debris. The flow-through was collected for SDS-PAGE analysis. The column was rigorously washed with lysis buffer (± 1 M NaCl and 15 mM imidazole). Proteins were eluted with a 100-500 mM imidazole gradient in lysis buffer. Wash and elution fractions were analysed by SDS-PAGE. The band representing ΔMICU is indicated by an arrow. (B) 0.2 and 2 µg of purified ΔMICU were transferred to a PVDF membrane. The membrane was blocked and probed with rabbit serum before and after rabbit immunization with ΔMICU. A secondary antibody conjugated with horse radish peroxidase was used to allow chemiluminescent detection of ΔMICU. (C) 20 µg of mitochondrial protein isolated from *35S:MICU.1:GFP*, Col-0, *micu-1* and *micu-2* seedlings according to Sweetlove et al., 2007 and Schwarzländer et al., 2011 were separated by SDS-PAGE and MICU was immunodetected as described in (B) using the purified MICU primary antibody instead of serum. Mitochondrially processed MICU and MICU.1:GFP were expected to have molecular masses of ~51 and ~81 kDa, respectively. The MICU.1:GFP band is indicated by an arrow.

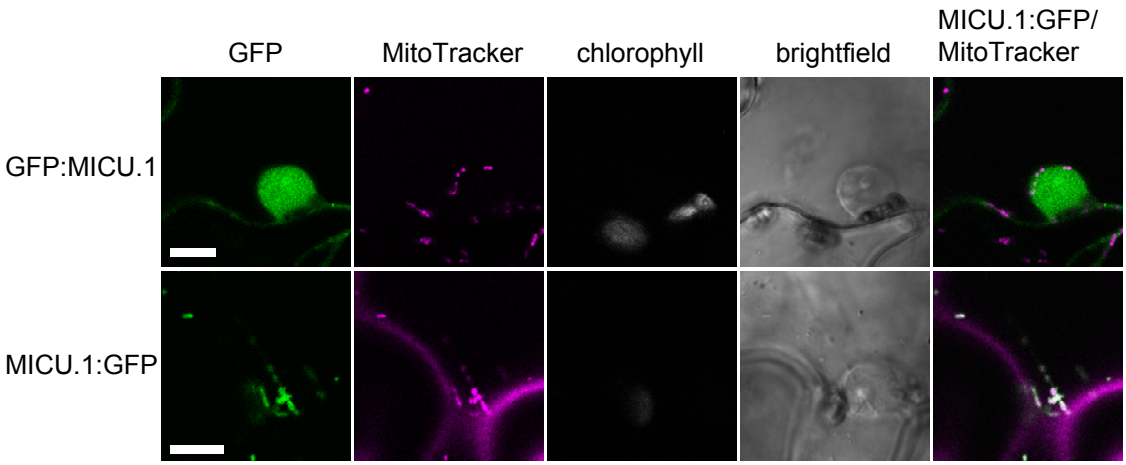

Supplemental Figure 3. MICU.1:GFP and GFP:MICU.1 localisation in wild tobacco leaf epidermis. *Nicotiana benthamiana* leaf epidermal cells transiently expressing GFP:MICU.1 and MICU.1:GFP stained with MitoTracker Orange and imaged by CLSM. GFP, green; MitoTracker, magenta. Scale bar = 10 µm.

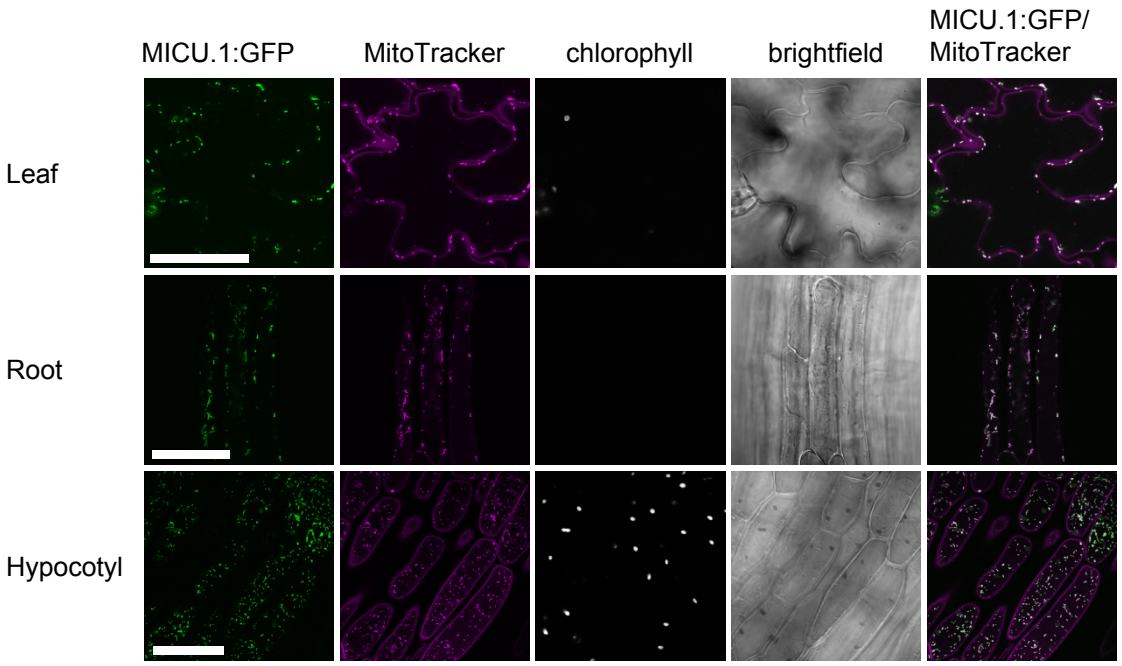

Supplemental Figure 4. Localisation of MICU.1:GFP in different *Arabidopsis* tissues. *Arabidopsis* seedlings stably expressing MICU.1:GFP and stained with MitoTracker Orange were imaged by CLSM. Representative images are shown for epidermal cells from the *Arabidopsis* leaf, root and hypocotyl. GFP, green; MitoTracker, magenta. Scale bar = 50 µm.

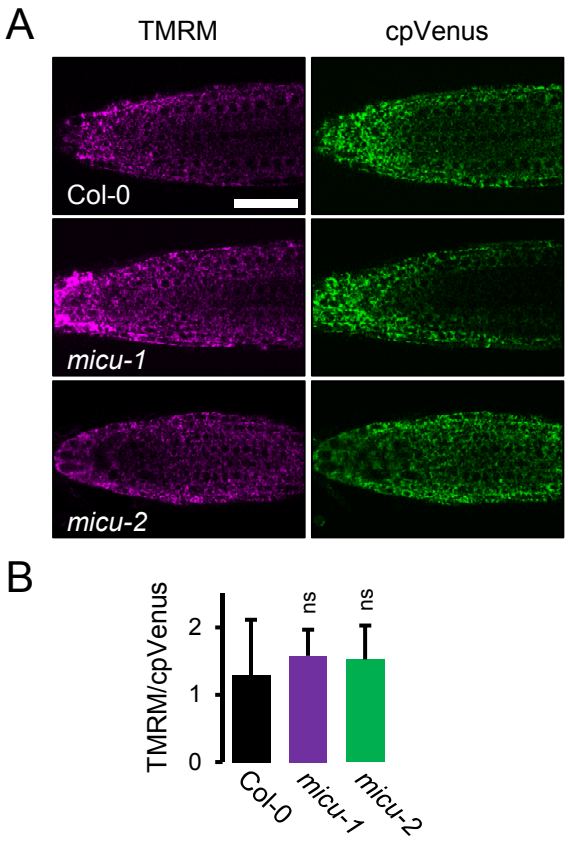

Supplemental Figure 5. Assessment of mitochondrial membrane potential in root tips. (A) Root tips expressing 4mt-YC3.6 equilibrated in 50 nM TMRM. Representative confocal images of TMRM (magenta) and cpVenus fluorescence intensity (green). Scale bar = 50 µm. (B) TMRM fluorescence intensity normalized over cpVenus fluorescence intensity from the ROI defined in **Figure 5C** is shown for the Col-0 (black), *micu-1* (purple) and *micu-2* (green) backgrounds. *n* = 5; error bars = SD. The pairwise comparisons (*micu vs.* wild-type; *t* test) indicated no significant (P ≤ 0.05) change (ns).

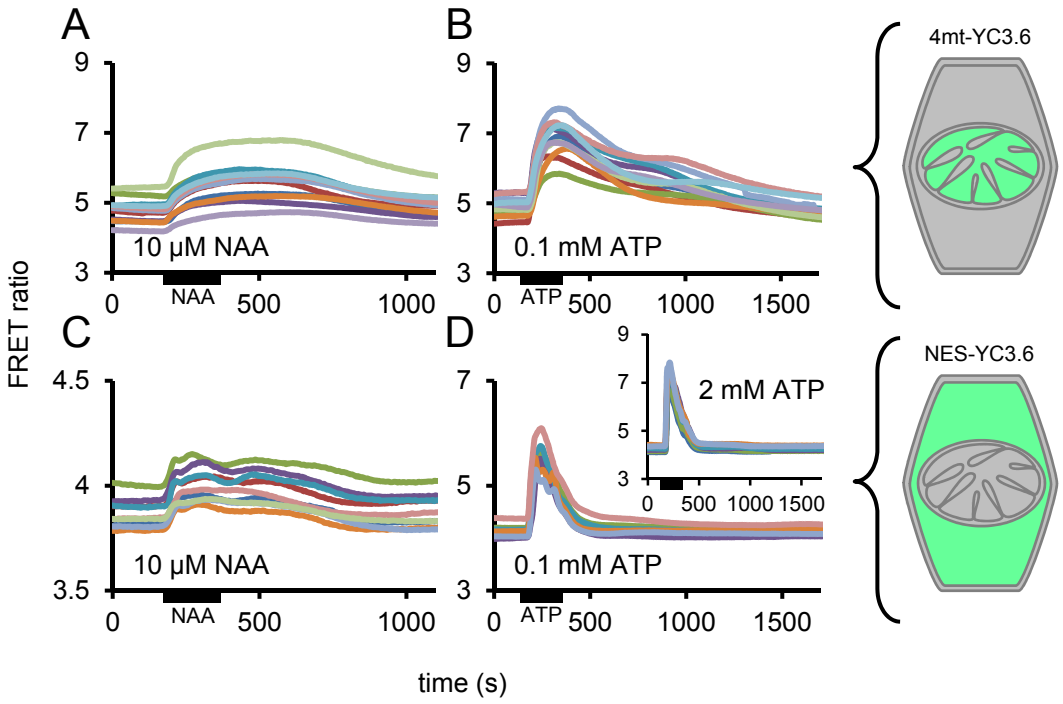

Supplemental Figure 6. Reproducibility of Ca^{2+} transients. FRET ratio traces of individual time lapse experiments of Col-0 seedlings expressing 4mt-YC3.6 (A and B) or NES-YC3.6 (C and D). Ca^{2+} transients were induced by the application of 10 µM NAA (A and C) or 0.1 mM ATP (B and D) at 175 s. The inset in (D) shows response traces for application of 2 mM ATP under otherwise identical conditions as for the main graph in (D). NAA and ATP were removed after another 180 s. (A) *n* = 11; (B) *n* = 11; (C) *n* = 9; (D) *n* = 8; insert in (D) *n* = 7.

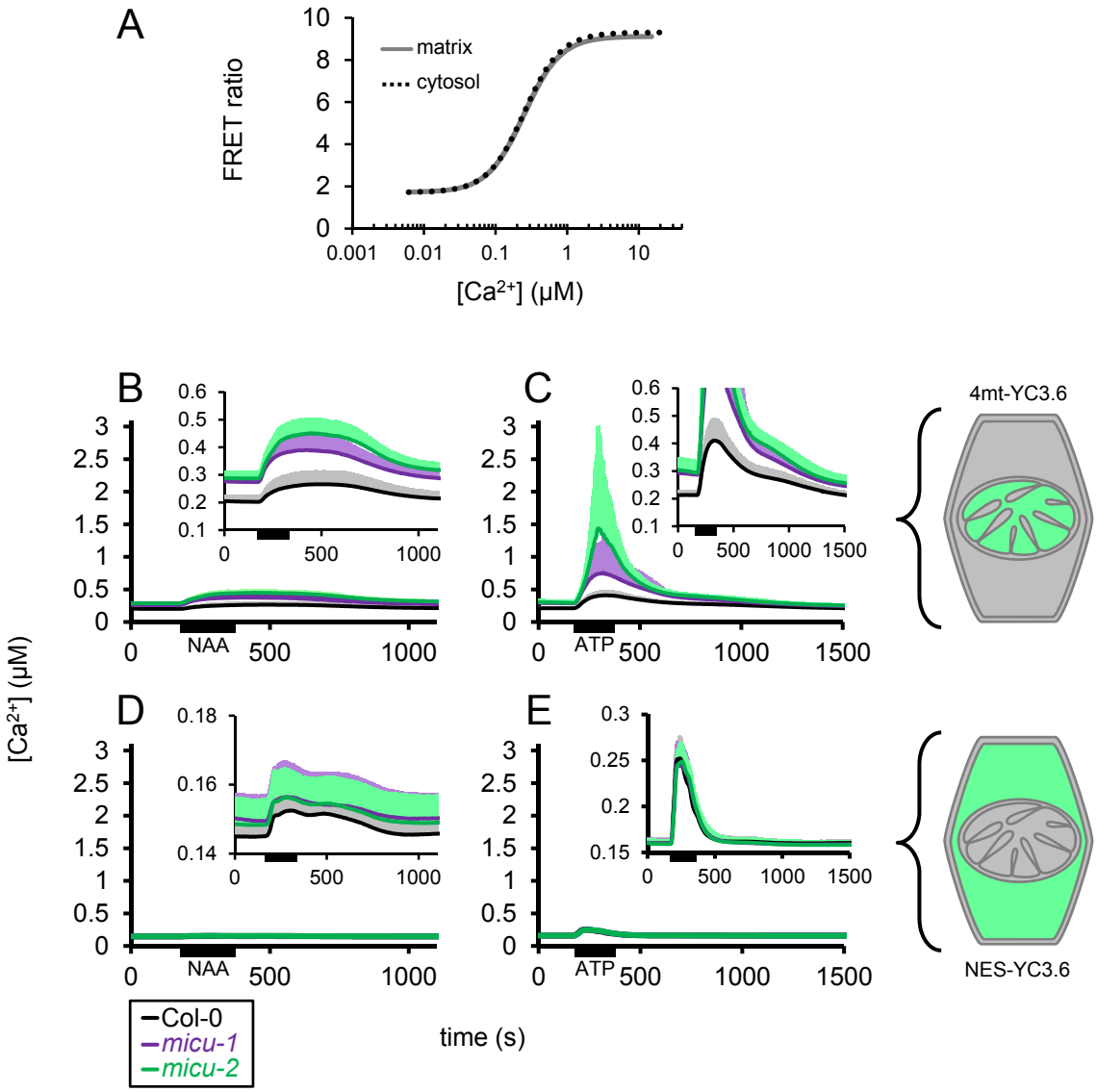

Supplemental Figure 7. Considerations on absolute free Ca^{2+} concentrations. (A) The YC3.6 sensor was calibrated based on the assumption of a matrix Ca^{2+} resting value of 208 nM in Col-0 (Logan and Knight, 2003) and *in vitro* sensor behaviour (K'_d: 250 nM, Hill coefficient: 1.7; Nagai et al., 2004; Palmer and Tsien, 2006) at pH 8.0 (assuming a dynamic range of 5.32) and pH 7.4 (dynamic range: 5.43) reflecting that of the mitochondrial matrix and the cytosol, respectively. Based on this approximation, free resting Ca^{2+} in the mitochondrial matrix of the *micu* lines is increased by > 35 % from 208 ± 22 nM in Col-0 to 287 ± 31 nM on average (B,C). The NAA-induced transients peak is >45% higher reaching 390 ± 58 nM in *micu-1* and 451± 57 nM in *micu-2* as compared to 266 ± 52 nM in Col-0 (B). The eATP-induced maximum is even more strongly increased reaching 758 ± 576 nM in *micu-1* and 1438 ± 1575 nM in *micu-2* as compared to 410 ± 82 nM in Col-0 (C). By comparison, cytosolic free Ca^{2+} can be estimated with 154 ± 9 nM at baseline and 155 ± 8 or 249 ± 98 nM at the NAA or eATP transient maximum in all lines. All estimates, with exception of the eATP-induced maxima in the *micu* matrix, are within the linear range of the sensor response. Non-linear effects are introduced by the relationship between sensor FRET ratio and free Ca^{2+} concentration, which is particularly pronounced when the sensor population is close to empty or fully occupied with Ca^{2+} (here: FRET ratio ranges < ~2.5 and > ~8.5). In that response region small changes in ratio are linked to large changes in free Ca^{2+} concentrations and the calculation of absolute free Ca^{2+} concentrations is particularly prone to error. By contrast, good correlation around the sensor K'_d (250 nM) validates quantitative assessment based on the FRET ratio data.

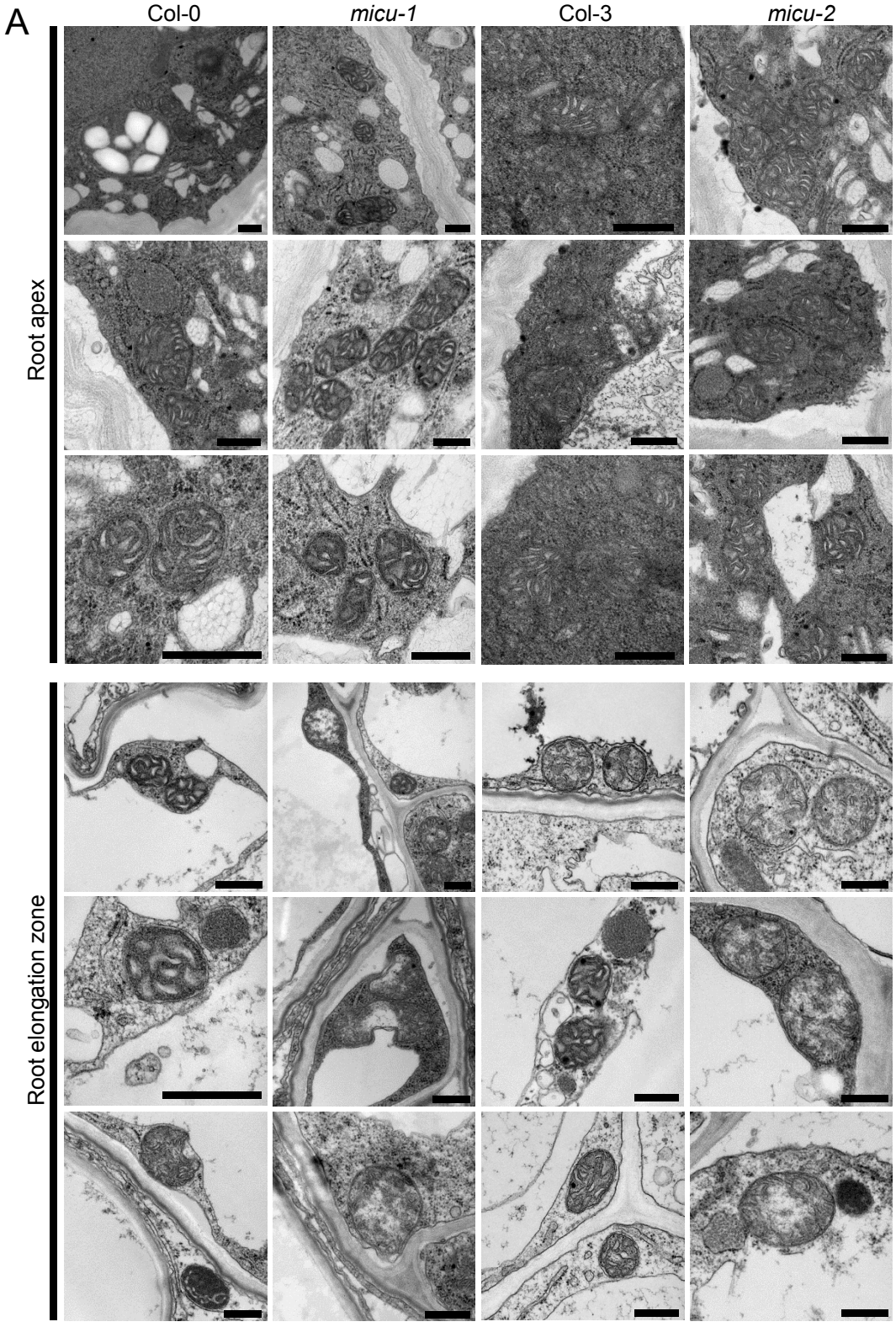

Supplemental Figure 8. Mitochondrial ultrastructure in cells of the root elongation zone and apex. (A) Mitochondrial ultrastructure in cells of the root apex and the elongation zone of *Arabidopsis* seedlings. Exemplary electron micrographs of *micu-1*, *micu-2* and their respective wild types (Col-0 and Col-3). Scale bars = 0.5 µm. Percentages of root apex mitochondria scored by matrix appearance are shown as a bar graph. ≥ 167 mitochondria from 3 different seedlings were scored per line. The analysis was repeated twice with consistent observations. ***P ≤ 0.001, ns: P > 0.01 (Chi-square test; **Supplemental Table 2)**.

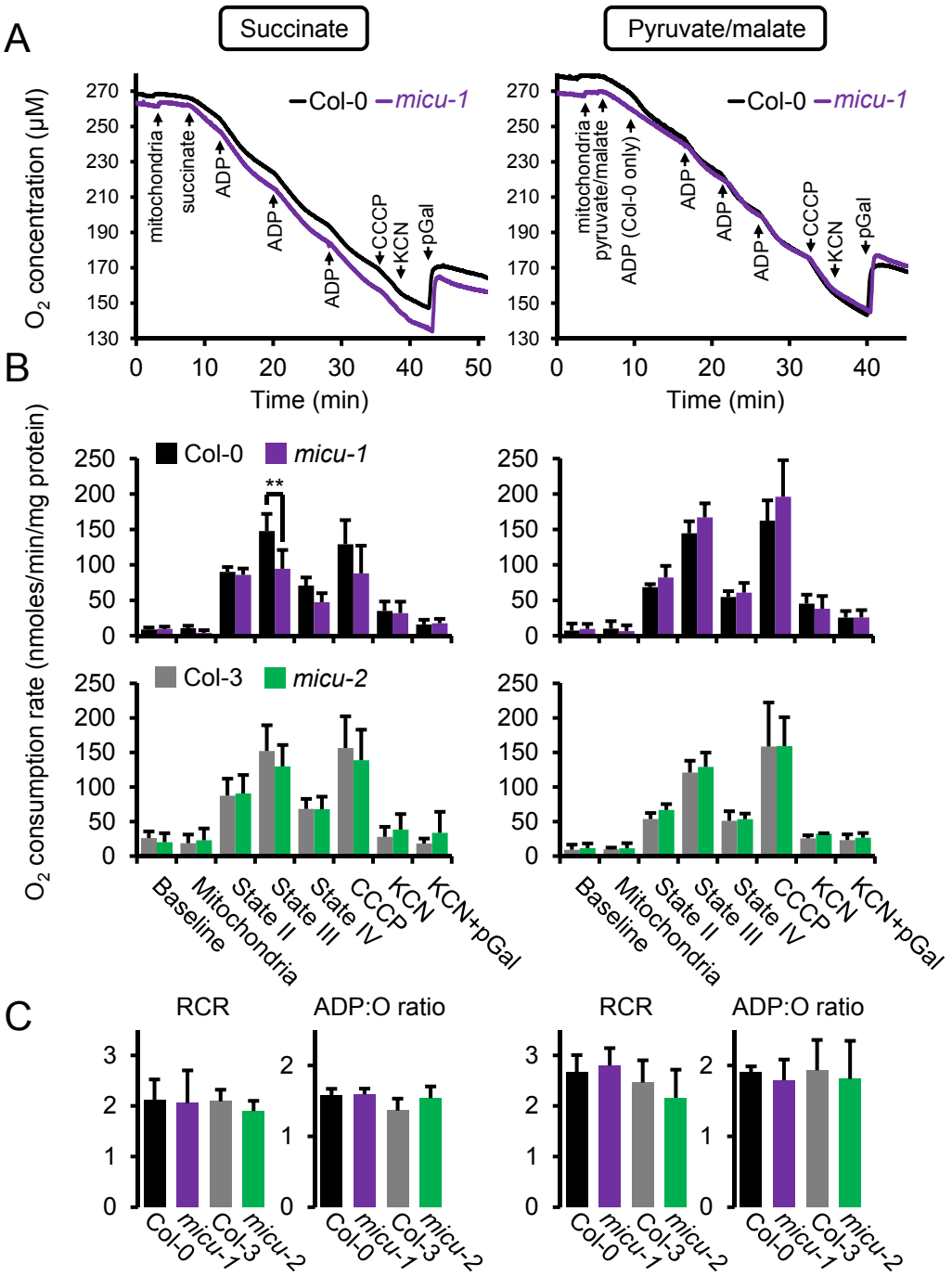

Supplemental Figure 9. Analysis of respiratory parameters in purified mitochondria. (A) Representative polarographic traces illustrating the oxygen consumption assays on purified mitochondria isolated from *Arabidopsis* seedlings, exemplified for Col-0 and *micu-1* energized with succinate or pyruvate/malate respectively. Additions are marked by arrows. Succinate: 10 mM succinate, 0.25 mM ATP; pyruvate/malate: 10 mM pyruvate, 10 mM malate, 0.3 mM NAD and 0.1 mM thiamine pyrophosphate; ADP: 50 µM ADP; CCCP: 10 µM carbonyl cyanide m-chlorophenylhydrazone; KCN: 1 mM KCN, 10 mM DTT, 2 mM pyruvate; pGal 0.2 mM propylgallate. (B) Oxygen consumption rates for purified mitochondria from Col-0 (black), *micu-1* (purple), Col-3 (grey), *micu-2* (green) energized with succinate or pyruvate/malate in response to the successive treatments indicated in (A). Outer membrane intactness was >90% for all preparations as measured by cytochrome *c* latency. (C) Respiratory control ratio (RCR; state IV rate/ state III rate) and ADP:O ratio (ADP or phosphate molecules consumed, or ATP molecules synthesized per consumed oxygen atom). *n* = 3 biological; error bars = SD. The statistical analysis (two way ANOVA with *post hoc* Holm-Sidak comparisons for *micu vs.* wild-type pairs) indicated no significant ($P \leq 0.05$) change, except in one case; **$P \leq 0.01$.

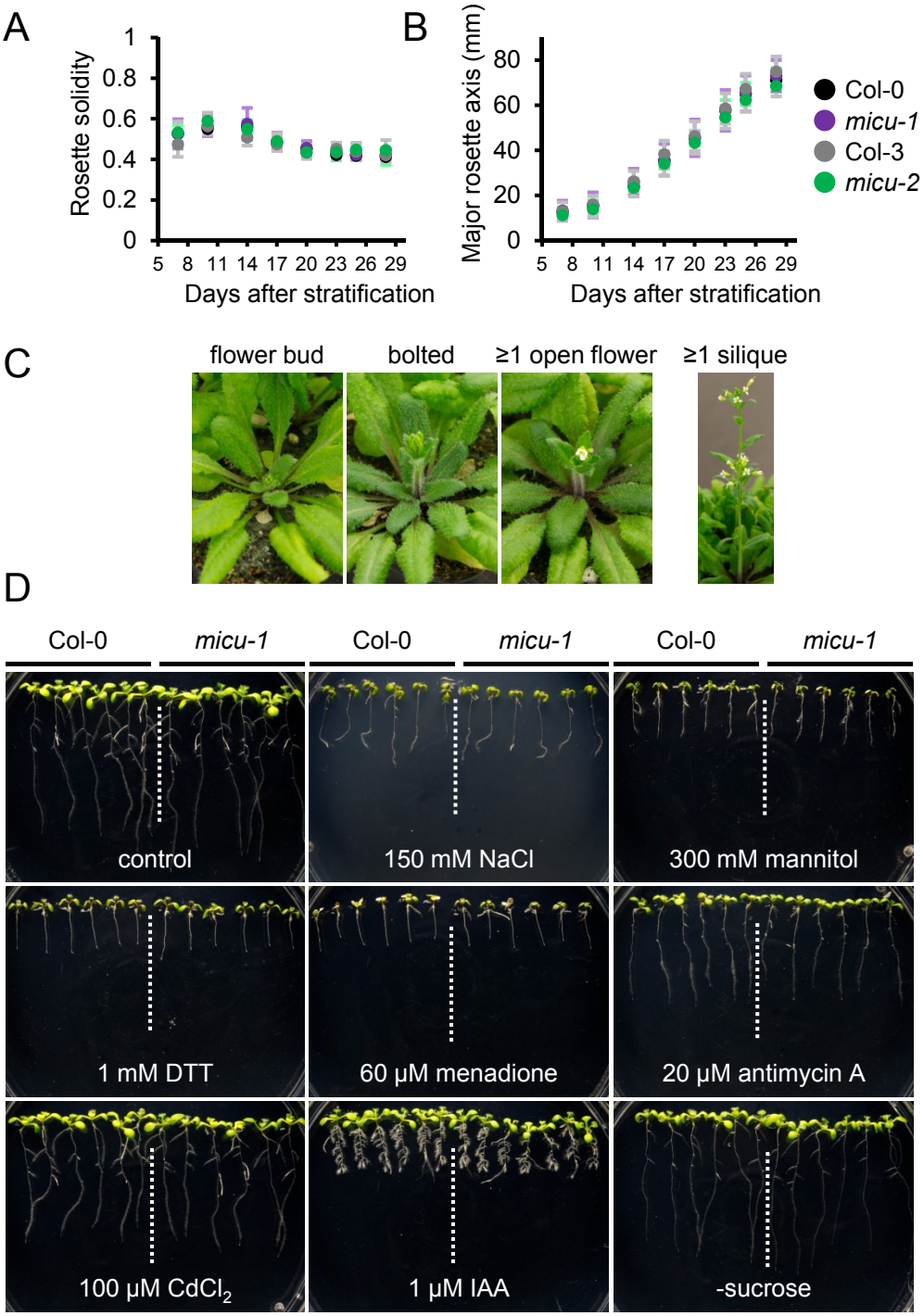

Supplemental Figure 10. Experimental design of *micu* phenotyping. Plants grown under controlled conditions were photographically documented in a standardised way using a Canon EOS 1000 D DSLR camera. For soil-grown rosettes the Leaf Lab tool (Version 1.41 b) was used to automatically detect rosette leaves and to quantify leaf area **(Fig. 8C)**, solidity (area of leaves in the rosette/ area of convex hull enclosing the rosette) and the length of the major rosette axis (A, B). (C) Representative images of plants in growth stages as classified in **Fig. 8D**. (D) Representative photographs of Col-0 and *micu-1* seedlings grown in the presence of a variety of additives and used for quantification of primary root length in **Fig. 8E**.

Supplemental Table 1. Kinetic parameters of cytosolic calcium transients in Col-0 and *micu* lines after stimulus with either NAA or eATP**.** $n \geq 7$; ± SD.

	NAA stimulus			**eATP stimulus**		
	Col-0	*micu-1*	*micu-2*	Col-0	*micu-1*	*micu-2*
Accumulation rate (ratio change s^{-1}) **(Fig. 7C,H)**	0.004 ±0.001	0.005 ±0.002	0.003 ±0.002	0.04 ±0.01	0.03 ±0.01	0.04 ±0.01
Maximal FRET ratio **(Fig. 7D,I)**	4.0 ±0.1	4.1 ±0.2	4.1 ±0.2	5.6 ±0.2	5.6 ±0.3	5.6 ±0.2
$t_{½\ up}$ (s)	26 ±5	23 ±4	24 ±9	21 ±4	25 ±7	24 ±7
$t_{½\ down}$ (s) **(Fig. 7E,J)**	516 ±45	486 ±64	471 ±133	329 ±8	348 ±15	347 ±25

Supplemental Table 2. Analysis of mitochondrial ultrastructure

Genotype	Root zone	Number of mitochondria			Percentage of mitochondria with translucent (abnormal) matrix	*p*-value χ^2 test
		scored	with dense (normal) matrix	with translucent (abnormal) matrix		
Col-0	Root apex	274	265	9	3.3	
micu-1	Root apex	255	254	1	0.4	0.015
Col-3	Root apex	268	257	11	4.1	
micu-2	Root apex	167	139	28	16.8	6.94E-06
Col-0	Elongation zone	235	202	33	14.0	
micu-1	Elongation zone	234	155	79	33.8	5.50E-07
Col-3	Elongation zone	185	142	43	23.2	
micu-2	Elongation zone	206	128	78	37.9	0.002

Supplemental Table 3. List of primers

Name	**Primer sequence**	**Purpose**
LBb1.3	ATTTTGCCGATTTCGGAAC	*micu-1* genotyping
P3054	GACAAGAATTAGGCAACAGG	*micu-1* genotyping
P3055	TAGACAAGGAGTTGGCCAC	*micu-1* genotyping
LB1mod	ATGGATAAATAGCCTTGCTTCC	*micu-2* genotyping
P3057	GATATGTCTGATACCGCGG	*micu-2* genotyping
P3058	TCCGAAGATGAATCCAGAGC	*micu-2* genotyping
P364	CAACCGGTATTGTGCTCGATTC	PCR reference gene *ACTIN7*
P436	AACCTCAGGACAACGGAATCTC	PCR reference gene *ACTIN7*
P2886	CGTCCGTTGACCGATCATTC	Validation of *MICU* knock-out through PCR
P2893	TCACGATGAGGAACAGTTCTTAG	Validation of *MICU* knock-out through PCR
P2455	CCATATTGCAAGAAGTTTGCGCGTCTG	qRT-PCR reference gene *SAND FAMILIY PROTEIN*
P2456	GCAAGTCATCGGGATGGAGAGACG	qRT-PCR reference gene *SAND FAMILIY PROTEIN*
P3529	GACCGATCATTCCTTCTCATC	Validation of *MICU* knock-out through qRT-PCR
P3530	CCAGAGGACCAATAGAGAAACC	Validation of *MICU* knock-out through qRT-PCR
P3389	GGGACATGCGTATCTCACTG	Validation of *MICU* knock-out through qRT-PCR
P3390	GCGGCTCGTTTGAAATCTT	Validation of *MICU* knock-out through qRT-PCR
ΔMICU_fw	TTTGCTAGCTCGTTTATTCCGAAATTGTC	Cloning of ΔMICU; NheI site is underlined
ΔMICU_rv	AAACTCGAGTCACGATGAGGAACAGTTCTTA	Cloning of ΔMICU; XhoI site is underlined

SUPPLEMENTAL REFERENCES

Edgar, R.C. (2004). MUSCLE: multiple sequence alignment with high accuracy and high throughput. Nucleic Acids Res **32,** 1792-1797.

Lewit-Bentley, A., and Rety, S. (2000). EF-hand calcium-binding proteins. Curr Opin Struct Biol **10,** 637-643.

Logan, D.C., and Knight, M.R. (2003). Mitochondrial and cytosolic calcium dynamics are differentially regulated in plants. Plant Physiol. **133,** 21-24.

Nagai, T., Yamada, S., Tominaga, T., Ichikawa, M., and Miyawaki, A. (2004). Expanded dynamic range of fluorescent indicators for Ca^{2+} by circularly permuted yellow fluorescent proteins. Proc Natl Acad Sci U S A **101,** 10554-10559.

Palmer, A.E., and Tsien, R.Y. (2006). Measuring calcium signaling using genetically targetable fluorescent indicators. Nat Protoc **1,** 1057-1065.

Perocchi, F., Gohil, V.M., Girgis, H.S., Bao, X.R., McCombs, J.E., Palmer, A.E., and Mootha, V.K. (2010). *MICU1* encodes a mitochondrial EF hand protein required for Ca^{2+} uptake. Nature **467,** 291-296.

Schwarzländer, M., Logan, D.C., Fricker, M.D., and Sweetlove, L.J. (2011). The circularly permuted yellow fluorescent protein cpYFP that has been used as a superoxide probe is highly responsive to pH but not superoxide in mitochondria: implications for the existence of superoxide 'flashes'. Biochem J **437,** 381-387.

Sweetlove, L.J., Taylor, N.L., and Leaver, C.J. (2007). Isolation of intact, functional mitochondria from the model plant *Arabidopsis thaliana*. Methods Mol Biol **372,** 125-136.